Excited-state nonlinear absorption in multi-energy-level molecular systems

Chunfei Li, Jinhai Si, Miao Yang, Ruibo Wang, and Lei Zhang
Department of Physics, Harbin Institute of Technology, Harbin 150001, China
(Received 4 March 1994; revised manuscript received 6 June 1994)

Three typical excited-state nonlinear absorption effects in molecular systems with weak ground-state absorption (at 532 nm) are experimentally demonstrated: (a) reverse saturable absorption (RSA) caused by strong triplet first-to-second excited-state absorption in a copper phthalocyanine solution with 15-ns laser pulses; (b) RSA caused by strong singlet first-to-second excited-state absorption in a C_{60} solution with 21-ps laser pulses; (c) the RSA-SA turnover caused by strong singlet first-to-second excited-state absorption and weak singlet second-to-third excited-state absorption in a metallo-porphyrin-like solution with 21-ps laser pulses. To simulate these excited-state nonlinear absorption behaviors we propose a general ten-level density-matrix model and its simplified models for the three cases. All simulations are in good agreement with the experimental results.

PACS number(s): 32.80.Rm, 33.80.Rv

I. INTRODUCTION

Nonlinear absorption means that the absorption coefficient of the medium depends on the light intensity, which is a fundamental nonlinear optical property. If the nonlinear absorption spectrum in a material is known, the nonlinear index of refraction in the material can be calculated in terms of the Kramers-Kronig relation and the nonlinear susceptibility $\chi^{(3)}$ can be determined. There are two kinds of nonlinear absorption in the single-photon process: saturable absorption (SA) and reverse saturable absorption (RSA), which have many important applications. SA in organic materials has been used for compressing laser pulses [1], and most dispersive optical bistable devices are based on the mechanism of SA [2]. However, such devices usually have large thermal loss and low throughput because they work on the peak of the linear absorption spectrum. In recent years, people have become interested in RSA, which shows promise in fabrication of devices for optical limiting [3], optical switching [4], and optical modulation [5]. These devices have many advantages, such as a fast response speed, a small linear absorption, a large transmission, and a mirrorless structure.

In principle, all energy levels in a molecular system contribute to the nonlinear absorption. The contribution of an energy level depends not only on the absorption cross section and lifetime but also on the incident laser pulse width and wavelength. In most studies, the wavelength is selected at a peak of the ground-state linear absorption spectrum of material. In this case, the absorption cross section of ground state is much greater than that of excited states, and the contribution of the ground-state absorption to the nonlinear absorption plays a dominant role. In this case, the molecular system exhibits SA.

There are many vibrational and rotational energy levels in organic molecular systems. Photons with the same wavelength can be simultaneously absorbed by molecules in the ground state as well as excited states. In the wavelength region off the peak of the ground-state linear absorption spectrum, and especially at the valley of that spectrum, the absorption cross section of the first excited state can be greater than that of the ground state. In this case, the first excited-state absorption becomes dominant and the molecular system exhibits RSA. The occurrence of RSA is due to two different mechanisms: if the laser pulse width is much longer than the intersystem-crossing lifetime (e.g., if ns pulses are used), the RSA is mainly attributed to the absorption of the triplet first excited state [6]; if the laser pulse width is much shorter than the intersystem-crossing lifetime (using ps pulses), the RSA is mainly attributed to the absorption of the singlet first excited state [7]. Actually, the higher excited states are also able to contribute to the nonlinear absorption. We will point out below that if the lifetime of the singlet second excited state is comparable to the ps laser pulse width, and the absorption cross section of the first excited state is greater than that of the ground state and the singlet second excited state, the material shows RSA in a lower light fluence range, which changes to SA at higher fluences, i.e., the turnover from RSA to SA appears in the material [8].

In this paper, we report experiments demonstrating three typical excited-state nonlinear absorption behaviors by measuring intensity-dependent transmissions of pulsed laser beams through three different materials, respectively. In order to simulate these experimental results, we propose a ten-level density-matrix model that takes into account the contribution of higher excited states to the nonlinear absorption. We also present three simplifications of the general model, one for each different system. Numerical simulations using these models are consistent with all experimental results. We describe excited-state nonlinear absorption behaviors in molecular systems by using a semiclassical density-matrix theory.

II. EXPERIMENTS

The following three materials were selected for investigation: C_{60}, copper phthalocyanine (CuPc), and cadmium

texaphyrin [(TXP)Cd]. The C_{60} molecule is a three-dimensional π-electron conjugated system having 60 π electrons distributed near both sides of the sphere-shape molecular surface. The CuPc and (TXP)Cd molecules are two-dimensional π-electron conjugated systems having 18 and 22 π electrons around the metal ion, respectively. The linear absorption spectra of these three materials including the ground-state absorption spectra and the excited-state differential absorption spectra are shown in Fig. 1(a) for C_{60} [9], Fig. 1(b) for CuPc [10], and Fig. 1(c) for (TXP)Cd [11], respectively. At the wavelength of 532 nm, their ground-state absorption is very weak; however, the singlet and triplet first excited-state absorption are quite strong. Therefore, RSA is expected in these materials at that wavelength.

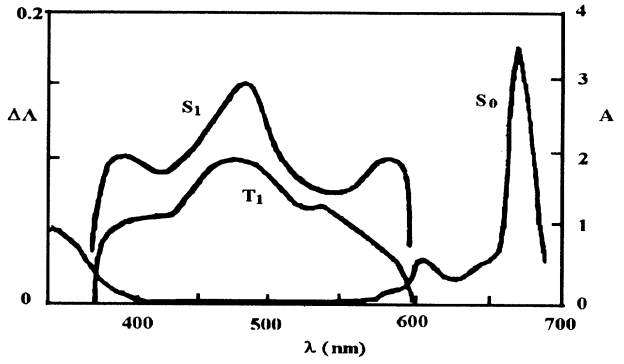

(a)

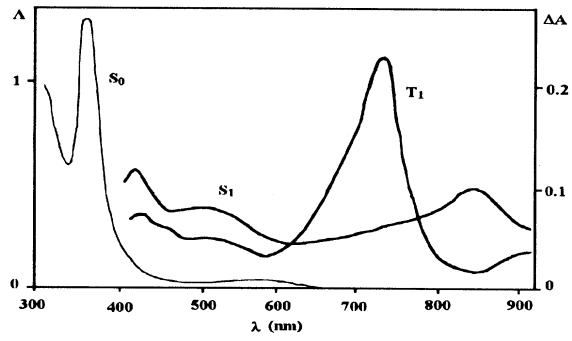

(b)

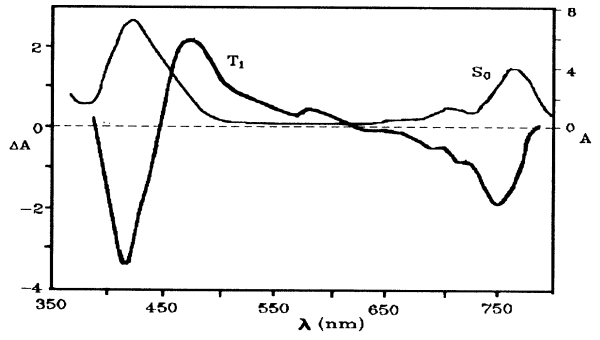

(c)

FIG. 1. Absorption spectra of the ground state and differential absorption spectra of excited states for (a) C_{60}, (b) CuPc, and (c) (TXP)Cd, respectively.

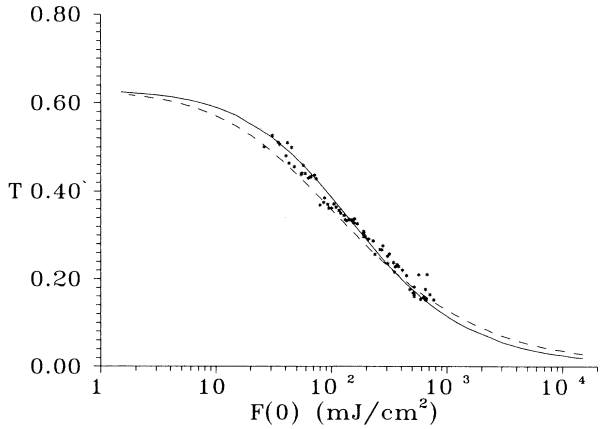

FIG. 2. Experimental data and theoretical curves of the energy transmittance vs the incident fluence for CuPc solution with 15-ns laser pulses. The solid curve comes from the dynamic theory and the dashed curve comes from the steady-state theory.

Nonlinear absorption measurements were made with a continuum Np70 Nd:YAG (yttrium aluminum garnet) laser system. The output beam from the laser system was frequency doubled to 532 nm and Q switched to 15 ns or mode locked to 21 ps with a repetition rate of ten times per second, and was focused into the sample cell by a 9-cm focal-length lens. The incident and output light energies were measured by two Rjp-735 energy detectors. Solvents, concentrations, linear transmittances, and path lengths of the three samples and laser pulse widths used in our experiments are all listed in Table I [6–8].

Experimental results of the energy transmittance T versus the incident fluence $F(0)$ for CuPc [6], C_{60} [7], and (TXP)Cd [8] are shown in Fig. 2, Fig. 3, and Fig. 4, respectively.

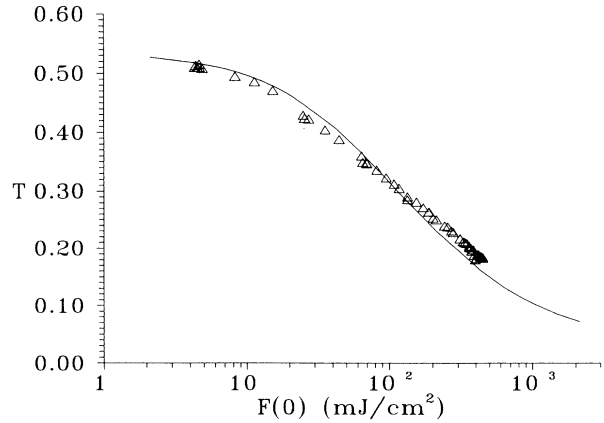

FIG. 3. Experimental data and the theoretical curve of the energy transmittance vs the incident fluence (the solid curve) for C_{60} with 21-ps laser pulses.

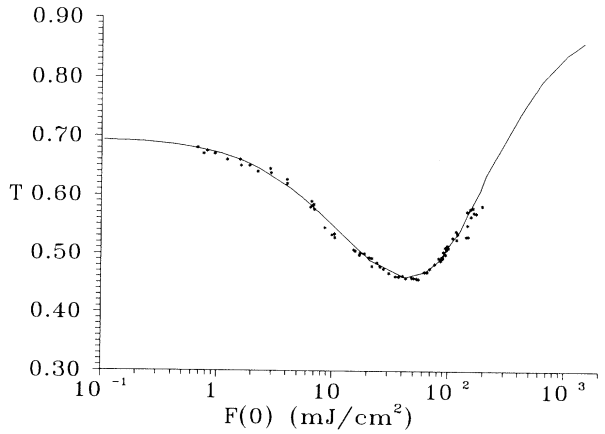

FIG. 4. Experimental data and the theoretical curve of the energy transmittance vs the incident fluence (the solid curve) for (TXP)Cd solution with 21-ps laser pulses.

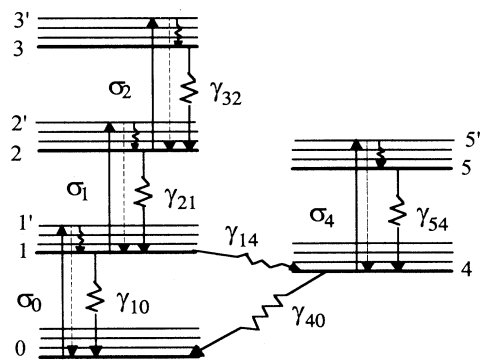

FIG. 5. Energy-level diagram for C_{60} and metallo-organic materials.

III. THEORETICAL MODEL

A schematic diagram of an energy-level system for C_{60} and the metallo-organic compounds is shown in Fig. 5, where 0 denotes the ground-state electronic level, and 1, 2, and 3 denote the singlet first, second, and third excited-state electronic level, respectively; 4 and 5 denote the triplet first and second excited-state electronic level, respectively. There are many sublevels above each electronic level, and i' denotes a sublevel of the ith excited-state electronic level.

When a molecular system is irradiated by a light beam with frequency ω, many molecules in the ground state are excited to the excited-state levels. The molecules in electronic levels 0, 1, 2, and 4 can simultaneously absorb incident photons with the same frequency ω and transit into the sublevels 1', 2', 3', and 5' of above next electronic levels with absorption cross sections σ_0, σ_1, σ_2, and σ_4, respectively. Because the lifetimes of molecules in those levels are very short, they relax rapidly with relaxation rate γ_{nm} back to the corresponding electronic levels, then transit to other levels. Let the eigenenergy and the eigenvalue of the level n be ε_n and $|n\rangle$, respectively, where $n=0,1,1',2,2',3,3',4,5,5'$, then the wave function and the unperturbed Hamiltonian of the molecular system can be written as

$$|\Psi\rangle=\sum_n c_n|n\rangle\ , \tag{1}$$

and

$$\hat{H}_0|n\rangle=\varepsilon_n|n\rangle\ . \tag{2}$$

The interaction Hamiltonian describing the interaction of light with the molecular system in the electric-dipole approximation is given by

$$\hat{H}_{\rm int}=-\hat{\mu}\cdot\mathbf{E}\ , \tag{3}$$

where $\hat{\mu}$ is electric-dipole operator and $\mathbf{E}$ is a monochromatic electric field, which can be expressed as

$$\mathbf{E}=\tfrac{1}{2}\mathbf{E}_0(t)\exp(-i\omega t)+\text{c.c.} \tag{4}$$

So the total Hamiltonian for the interaction between a light and a ten-level molecular system can be written as

$$\hat{H}=\hat{H}_0+\hat{H}_{\rm int}\ . \tag{5}$$

The matrix expression of $\hat{H}$ is

$$\hat{H}=\begin{pmatrix}
\varepsilon_0 & 0 & -\mu_{01'}E & 0 & 0 & 0 & 0 & -\mu_{04}E & 0 & 0\\
0 & \varepsilon_1 & 0 & 0 & -\mu_{12'}E & 0 & 0 & 0 & 0 & 0\\
-\mu_{1'0}E & 0 & \varepsilon_{1'} & 0 & 0 & 0 & 0 & 0 & 0 & 0\\
0 & 0 & 0 & \varepsilon_2 & 0 & 0 & -\mu_{23'}E & 0 & 0 & 0\\
0 & -\mu_{2'1}E & 0 & 0 & \varepsilon_{2'} & 0 & 0 & 0 & 0 & 0\\
0 & 0 & 0 & 0 & 0 & \varepsilon_3 & 0 & 0 & 0 & 0\\
0 & 0 & 0 & 0 & -\mu_{3'2}E & 0 & \varepsilon_{3'} & 0 & 0 & 0\\
-\mu_{40}E & 0 & 0 & 0 & 0 & 0 & 0 & \varepsilon_4 & 0 & -\mu_{45'}E\\
0 & 0 & 0 & 0 & 0 & 0 & 0 & 0 & \varepsilon_5 & 0\\
0 & 0 & 0 & 0 & 0 & 0 & 0 & -\mu_{5'4}E & 0 & \varepsilon_{5'}
\end{pmatrix}\ . \tag{6}$$

TABLE I. Experimental parameters of samples and laser pulse widths.

Sample	Solvent	Concentration	Transmittance	Path length	Pulse width
C_{60}	toluene	7.2×10^{-4} M	54%	5 mm	21 ps
CuPc	chloroform	7.5×10^{-4} M	63%	5 mm	15 ns
(TXP)Cd	chloroform	2.3×10^{-4} M	70%	2 mm	21 ps

The density-matrix operator is defined as

$$\hat{\rho}=|\Psi\rangle\langle\Psi| , \tag{7}$$

and the equation of motion for $\hat{\rho}$ (Liouville equation) is

$$\frac{\partial\hat{\rho}}{\partial t}=\frac{1}{i\hbar}[\hat{H},\hat{\rho}] . \tag{8}$$

Equation (8) can also be expressed as

$$\frac{\partial\rho_{nm}}{\partial t}=\frac{1}{i\hbar}\sum_{k}(H_{nk}\rho_{km}-\rho_{nk}H_{km}) . \tag{9}$$

Using Eqs. (6) and (9) and considering the relaxation of each state, the equations of motion for density-matrix elements can be obtained,

$$\begin{aligned}
&\frac{\partial\rho_{1'0}}{\partial t}=-i\omega_{1'0}\rho_{1'0}+\frac{i\mu_{1'0}}{\hbar}(\rho_{00}-\rho_{1'1'})E-\Gamma_{1'0}\rho_{1'0} ,\\
&\frac{\partial\rho_{2'1'}}{\partial t}=-i\omega_{2'1'}\rho_{2'1'}+\frac{i\mu_{2'1}}{\hbar}(\rho_{11}-\rho_{2'2'})E-\Gamma_{2'1}\rho_{2'1} ,\\
&\frac{\partial\rho_{3'2}}{\partial t}=-i\omega_{3'2}\rho_{3'2}+\frac{i\mu_{3'2}}{\hbar}(\rho_{22}-\rho_{3'3'})E-\Gamma_{3'2}\rho_{3'2} ,\\
&\frac{\partial\rho_{5'4}}{\partial t}=-i\omega_{5'4}\rho_{5'4}+\frac{i\mu_{5'4}}{\hbar}(\rho_{44}-\rho_{5'5'})E-\Gamma_{5'4}\rho_{5'4} ,\\
&\frac{\partial\rho_{11}}{\partial t}=-\frac{i\mu_{2'1}}{\hbar}E(\rho^{*}_{2'1}-\rho_{2'1})+\gamma_{1'1}\rho_{1'1'}-(\gamma_{10}+\gamma_{14})\rho_{11} ,\\
&\frac{\partial\rho_{1'1'}}{\partial t}=\frac{i\mu_{1'0}}{\hbar}E(\rho^{*}_{1'0}-\rho_{1'0})-\gamma_{1'1}\rho_{1'1'} ,\\
&\frac{\partial\rho_{22}}{\partial t}=-\frac{i\mu_{3'2}}{\hbar}E(\rho^{*}_{3'2}-\rho_{3'2})+\gamma_{2'2'}\rho_{2'2'}-\gamma_{21}\rho_{22}+\gamma_{32}\rho_{33} ,
\end{aligned} \tag{10}$$

$$\begin{aligned}
&\frac{\partial\rho_{2'2'}}{\partial t}=\frac{i\mu_{2'1}}{\hbar}E(\rho^{*}_{2'1}-\rho_{2'1})-\gamma_{2'2'}\rho_{2'2'} ,\\
&\frac{\partial\rho_{33}}{\partial t}=\gamma_{3'3}\rho_{3'3'}-\gamma_{32}\rho_{33} ,\\
&\frac{\partial\rho_{3'3'}}{\partial t}=\frac{i\mu_{3'2}}{\hbar}E(\rho^{*}_{3'2}-\rho_{3'2})-\gamma_{3'3}\rho_{3'3'} ,\\
&\frac{\partial\rho_{44}}{\partial t}=-\frac{i\mu_{5'4}}{\hbar}E(\rho^{*}_{5'4}-\rho_{5'4})+\gamma_{14}\rho_{11}+\gamma_{54}\rho_{55}-\gamma_{40}\rho_{44} ,\\
&\frac{\partial\rho_{55}}{\partial t}=\gamma_{5'5'}\rho_{5'5'}-\gamma_{54}\rho_{55} ,\\
&\frac{\partial\rho_{55'}}{\partial t}=\frac{i\mu_{54}}{\hbar}E(\rho^{*}_{54}-\rho_{5'4})-\gamma_{55}\rho_{55'} .
\end{aligned}$$

Here, Γ_{nm} and γ_{nm} are the transverse relaxation rate and the longitudinal relaxation rate, respectively.

Multiplying both sides of the off-diagonal matrix element equations in Eq. (10) by $\exp[(i\omega_{nm}+\Gamma_{nm})t]$ and integrating it, we can obtain

$$\begin{aligned}
\rho_{nm}=\frac{i\mu_{nm}}{2\hbar}\int_{-\infty}^{t}dt'\exp[-(i\omega_{nm}+\Gamma_{nm})(t-t')]\\
\times[E_0(t)\exp(-i\omega t')+\text{c.c.}]\\
\times(\rho_{mm}-\rho_{nn}) .
\end{aligned} \tag{11}$$

Assuming that the amplitude $E_0(t)$ of the electric field and the population ρ_{mm} of $|m\rangle$ state are slowly varying functions, which can be factored outside the integral, the only remaining term is $\exp(-i\omega t)$. Hence, from Eq. (11), we obtain

$$\rho_{nm}=\frac{i\mu_{nm}}{2\hbar}E_0(t)\exp(-i\omega t)\frac{(\rho_{mm}-\rho_{nn})}{\Gamma_{nm}+i(\omega-\omega_{nm})} . \tag{12}$$

Substituting ρ^{*}_{nm} and ρ_{nm} into the diagonal matrix elements equations, we have

$$\frac{\partial\rho_{mm}}{\partial t}=-\frac{i\mu_{nm}}{\hbar}E(\rho^{*}_{nm}-\rho_{nm})+\cdots ,$$

which yields

$$\begin{aligned}
\frac{\partial\rho_{mm}}{\partial t}=\frac{\mu^{2}_{nm}}{2\hbar^{2}}|E_0(t)|^{2}\frac{\Gamma_{nm}}{\Gamma^{2}_{nm}+(\omega_{nm}-\omega)^{2}}(\rho_{mm}-\rho_{nn})\\
+\cdots .
\end{aligned} \tag{13}$$

Because $I=\frac{1}{2}cn\varepsilon_0|E_0(t)|^{2}$, where ε_0 is the electric permeability, and defining the absorption cross section from $|m\rangle$ state to $|n\rangle$ state as

$$\sigma_{mn}=\frac{\omega\Gamma_{nm}\mu^{2}_{nm}}{\hbar nc\varepsilon_0[\Gamma^{2}_{nm}+(\omega_{nm}-\omega)^{2}]} , \tag{14}$$

Eq. (13) can be written as

$$\frac{\partial\rho_{mm}}{\partial t}=-\sigma_{mn}\phi(\rho_{mm}-\rho_{nn})+\cdots , \tag{15}$$

where $\phi=I/\hbar\omega=cn\varepsilon_0|E_0(t)|^{2}/2\hbar\omega$ is the photon flux. Because lifetimes of three and five electronic levels and lifetimes of all of sublevels are very short, we assume that $\rho_{11'}=\rho_{2'2'}=\rho_{3'3'}=\rho_{5'5'}=\rho_{33}=\rho_{55}=0$. Using Eq. (15), equations for diagonal matrix elements can be written as

$$\frac{\partial\rho_{11}}{\partial t}=\sigma_0\phi\rho_{00}-\sigma_1\phi\rho_{11}-(\gamma_{10}+\gamma_{14})\rho_{11}+\gamma_{21}\rho_{22}\ ,$$
$$\frac{\partial\rho_{22}}{\partial t}=\sigma_1\phi\rho_{11}-\sigma_2\phi\rho_{22}-\gamma_{21}\rho_{22}+\gamma_{32}\rho_{33}\ ,$$
$$\frac{\partial\rho_{44}}{\partial t}=-\sigma_4\phi\rho_{44}+\gamma_{14}\rho_{11}+\gamma_{54}\rho_{55}-\gamma_{40}\rho_{44}\ , \tag{16}$$
$$\rho_{00}+\rho_{11}+\rho_{22}+\rho_{44}=1\ .$$

Furthermore, we should consider a light-propagation equation

$$\frac{\partial\phi}{\partial z}=-(\sigma_0\rho_{00}+\sigma_1\rho_{11}+\sigma_2\rho_{22}+\sigma_4\rho_{44})N\phi\ , \tag{17}$$

where $\sigma_0=\sigma_{01}$, $\sigma_1=\sigma_{12}$, $\sigma_2=\sigma_{23}$, $\sigma_4=\sigma_{45}$, and N is the total molecular number density.

We also establish the initial and boundary conditions as follows:

$$\rho_{11}(t=-\infty,z)=1\ ,$$
$$\rho_{22}(t=-\infty,z)=\rho_{33}(t=-\infty,z)$$
$$=\rho_{44}(t=-\infty,z)=0\ , \tag{18}$$
$$\phi(t,z=0)=\frac{1}{\hbar\omega}I_0(z=0)\exp\left[-c\left[\frac{t}{t_L}\right]^2\right]\ ,$$

where $I_0(z=0)$ is the peak intensity of the incident laser pulse and t_L is the laser pulse width. The pulse is assumed to be with a Gaussian temporal profile, and c is a normalized constant coefficient.

IV. SIMULATIONS

Photophysical parameters used in the simulation of the three materials, which correspond to solutions of C_{60} in toluene, CuPc, and (TXP)Cd in chloroform, are summarized in Table II, where $\tau_1=(\gamma_{10}+\gamma_{14})^{-1}$, $\tau_2=\gamma_{21}^{-1}$, $\tau_4=\gamma_{40}$.

Substituting the data in Tables I and II into Eqs. (16)–(18), the experimental results described in Sec. III can be simulated by calculating numerically T-$F(0)$ curves. To simplify the calculations, we reduce Eqs. (16) and (17) to a simplified form for the following three cases.

TABLE II. Photophysical parameters of C_{60}, CuPc, and (TXP)Cd solutions.

Sample	C_{60}	CuPc	(TXP)Cd
σ_0 (cm^2)	2.87×10^{-18}	2.0×10^{-18}	2.45×10^{-17}
σ_1 (cm^2)	1.57×10^{-17}	3.5×10^{-17}[a]	1.0×10^{-16}[a]
σ_2 (cm^2)			3.0×10^{-18}[a]
σ_4 (cm^2)	9.22×10^{-18}	2.6×10^{-17}[a]	3.5×10^{-17}[a]
τ_1 (ns)	1	0.1	0.1
τ_2 (ps)			4.7[a]
τ_4 (μs)	280	<0.05	22
Ref.	[9]	[12]	[11]

[a]Denotes parameters that are determined by fitting theoretical simulations with our experimental results.

A. Simulations of reverse saturable absorption in CuPc

Because the lifetimes of level 2, 3, and 5 are very short ($\leq$ps), we let $\rho_{22}=0$, $\sigma_1\phi\rho_{11}=\gamma_{21}\rho_{22}$, and $\sigma_4\phi\rho_{44}=\gamma_{54}\rho_{55}$. Equations (16) and (17) can then be written as

$$\frac{\partial\rho_{11}}{\partial t}=\sigma_0\phi\rho_{00}-(\gamma_{10}+\gamma_{14})\rho_{11}\ ,$$
$$\frac{\partial\rho_{44}}{\partial t}=\gamma_{14}\rho_{11}-\gamma_{40}\rho_{44}\ , \tag{19}$$
$$\rho_{00}+\rho_{11}+\rho_{44}=1\ ,$$

and

$$\frac{\partial\phi}{\partial z}=-(\sigma_0\rho_{00}+\sigma_1\rho_{11}+\sigma_4\rho_{44})N\phi\ . \tag{20}$$

Equations (19) and (20) describe a three-level molecular model. In this case, the laser pulse width of 15 ns is much longer than the intersystem-crossing lifetime of 0.1 ns, most molecules quickly transit from level 1 to 4. Then there is a strong absorption of the incident photons by molecules in the triplet first excited state, and we can let $\rho_{11}\approx0$ and $\partial\rho_{11}/\partial t=0$. Because $\gamma_{10}\ll\gamma_{14}$, γ_{10} can also be neglected. Then, Eqs. (19) and (20) can be further simplified to

$$\frac{\partial\rho_{44}}{\partial t}=\sigma_0\phi-(\sigma_0\phi+\gamma_{40})\rho_{44}\ ,$$
$$\rho_{00}+\rho_{44}=1\ , \tag{21}$$
$$\frac{\partial\phi}{\partial z}=-[\sigma_0-(\sigma_0-\sigma_4)\rho_{44}]N\phi\ .$$

Using Eqs. (21) and (18), we have calculated the T-$F(0)$ theoretical curve, which is the solid line in Fig. 2. It shows good agreement between the theoretical curve and the experimental data.

From Table I, it can be seen that the lifetime of the first triplet state of CuPc is very short ($\tau_4<50$ ns). Because of triplet-triplet state annihilation at high concentration and triplet state annihilation reaction by oxygen, the lifetime τ_4 of CuPc solution (≈10 ns) can be shorter than the laser pulse width τ_L (15 ns); therefore, the steady-state theory can be used. Assuming $\partial/\partial t=0$, Eq. (21) yields

$$\rho_{00}=\frac{1}{1+I'}\ ,\quad \rho_{44}=\frac{I'}{1+I'}\ , \tag{22}$$

where $I'=I/I_s$. I_s is the saturable intensity, which is defined as $I_s=\hbar\omega/\tau_4\sigma_0$ and $\tau_4=1/\gamma_{40}$. Substituting Eq. (22) into the light-propagation equation, we obtain

$$\ln\left[\frac{T}{T_0}\right]=\left[1-\frac{1}{k}\right]\ln\left[\frac{1+kTI_0'}{1+kI_0'}\right]\ , \tag{23}$$

where $k=\sigma_4/\sigma_0$, $T=I(L)/I(0)$, T_0 is the linear transmittance, and L is the thickness of sample. Using Eq. (23) and taking $T_0=0.6$, $K=13$, and $I_s=2\times10^7$ W/cm^2, the steady-state RSA curve for CuPc has been calculated as shown in Fig. 2 (dashed line), which is also consistent with the experimental data.

B. Simulations of reverse saturable absorption in C_{60}

When the laser pulse width is 21 ps, it is shorter than the intersystem-crossing lifetime of 1 ns and much shorter than the singlet first excited-state lifetime τ_1. Therefore, the nonlinear absorption for C_{60} must be treated by the dynamic theory, and we can let $\partial\rho_{44}/\partial t=0$, $\rho_{44}=0$, and $\gamma_1=\gamma_{10}+\gamma_{14}$. Then Eqs. (19) and (20) can be simplified into

$$\begin{aligned}&\frac{\partial\rho_{44}}{\partial t}=\sigma_0\phi-(\sigma_0\phi+\gamma_1)\rho_{44}\ ,\\&\rho_{00}+\rho_{44}=1\ ,\\&\frac{\partial\phi}{\partial z}=-[\sigma_0-(\sigma_0-\sigma_1)\rho_{11}]N\phi\ .\end{aligned}\tag{24}$$

Using (24) we have calculated the T-$F(0)$ theoretical curve as shown in Fig. 3 (solid line), which is in agreement with the experimental results.

C. RSA-SA simulation for (TXP)Cd

Because the laser pulse width of 21 ps is much shorter than the intersystem-crossing lifetime of about 0.1 ns, we let $\rho_{44}=0$. The contribution of the singlet second excited state to nonlinear absorption cannot be neglected, because it has a longer lifetime (4.7 ps) comparable to the laser pulse width. We can use a singlet-four-level model, which is described by the following equations:

$$\begin{aligned}&\frac{\partial\rho_{11}}{\partial t}=\rho_0\phi-(\sigma_0\phi+\sigma_1\phi+\gamma_1)\rho_{11}-(\sigma_0\phi-\gamma_{21})\rho_{22}\ ,\\&\frac{\partial\rho_{22}}{\partial t}=\sigma_1\phi\rho_{11}-\gamma_{21}\rho_{22}\ ,\\&\rho_{00}+\rho_{11}+\rho_{22}=1\ ,\\&\frac{\partial\phi}{\partial z}=-[\sigma_0-(\sigma_0-\sigma_1)\rho_{11}-(\sigma_0-\sigma_2)\rho_{22}]N\phi\ .\end{aligned}\tag{25}$$

The theoretical simulation of the nonlinear absorption for (TXP)Cd is shown in Fig. 4 (solid curve). One can see that RSA is turned into SA at fluences higher than 40 mJ/cm^2. In other words, the RSA occurs at low fluences and SA occurs at high fluences.

We should mention here that some photophysical parameters of the singlet second excited state, such as absorption cross section and lifetime, were evaluated by fitting the theoretical curves with the experimental data.

V. CONCLUSIONS

Three different excited-state nonlinear absorption processes in two-dimensional and three-dimensional π-electron conjugated molecular systems under the action of laser pulses were studied experimentally and theoretically. A density-matrix model for a ten-level molecular system was proposed and an approximation of laser pulse with the Gaussian-shaped temporal profile was used. Diagonal density-matrix element equations were simplified into simpler rate-equation groups for three different cases. Good agreement between simulations and experiments show that these models are correct.

The results show that whether the excited-state nonlinear absorption displays RSA or SA mainly depends on the absorption cross section and the lifetime of energy levels of the molecule and on the pulse width of incident laser.

If incident laser pulse width is not very short, the contribution of higher excited states to the nonlinear absorption can be neglected. In this situation, if $\sigma_0>\sigma_1$ and σ_4, the system exhibits SA; if σ_1 or/and $\sigma_4>\sigma_0$, the system exhibits RSA.

The contributions of triplet and singlet first excited states to the RSA are different, and depend on the comparison between the laser pulse width τ_L and the intersystem-crossing time τ_{14}. If $\tau_L>\tau_{14}$, the contribution of the singlet first-excited state is dominant; if $\tau_L<\tau_{14}$, the contribution of the triplet first excited state is dominant.

If the laser pulse width is shorter than the lifetime of the singlet second excited state, the nonlinear absorption property of material could be changed with increasing the light fluence: if $\sigma_2<\sigma_1>\sigma_0$, the turnover is from RSA to SA; if $\sigma_2>\sigma_1<\sigma_0$, the turnover is from SA to RSA.

If the laser pulse width is longer than all energy-level lifetimes, the steady-state theory could be used. Otherwise the dynamic theory should be used.

Now we have more understanding of the excited-state nonlinear absorption in multi-energy-level systems, which belongs to a new field of nonlinear optics called "excited-state nonlinear optics." The excited-state nonlinear absorption can be applied in the photonic technology to make high transparent ultrafast photonic devices for optical limiting, optical switching, and optical modulation [4].

ACKNOWLEDGMENTS

The authors are grateful to Dr. Hui Wang, Feng-Yun Guo, Ying-Lin Song, and Yu-Xiao Wang for their help in some calculations and experiments. This research work was supported by the National Natural Science Foundation of China.

[1] W. F. Kosonpcky and S. E. Harrison, J. Appl. Phys. **37**, 4789 (1966).
[2] H. M. Gibbs, *Optical Bistability: Controlling with Light* (Academic, New York, 1985).
[3] L. W. Tutt, and S. W. McCahon, Opt. Lett. **15**, 700 (1990).
[4] Chun-Fei Li, Miao Yang, Fengyun Guo, Yuxiao Wang, and Kuna Tada, Int. J. Nonlinear Opt. Phys. **2**, 551 (1993).
[5] K. W. Beeson, J. T. Yardley, and S. Speiser, Proc. SPIE

1337, 364 (1990).
[6] Chun-Fei Li, Lei Zhang, Miao Yang, Hui Wang, and Yu-Xiao Wang, Phys. Rev. A **49**, 1149 (1994).
[7] Chen-Fei Li, Yuxiao Wang, Feng-Yun Guo, Rui-Bo Wang, and Lei Zhang, J. Opt. Soc. Am. B **11**, 8 (1994).
[8] Jin-Hai Si, Miao Yang, Yu-Xiao Wang, Lei Zhang, and Chun-Fei Li, Appl. Phys. Lett. **64**, 23 (1994).
[9] T. W. Ebbesen, K. Tanigaki, and S. Kuroshima, Chem. Phys. Lett. **181**, 501 (1991).
[10] Hiroyuki Ohtanl, Takayoshi Kobayashi, Takeshi Ohno, Shunji Kato, Takshi Tanno, and Akira Yamada, J. Phys. Chem. **88**, 18 (1984).
[11] B. G. Maiya, A. Harriman, J. L. Sessler, G. Hemmi, T. Murai, and T. E. Mallouk, J. Phys. Chem. **93**, 8111 (1989).
[12] M. Hercher, W. Chu, and D. L. Stockman, IEEE J. Quantum Electron. **QE-4**, 954 (1986).